

Know your building blocks: time-resolved EPR spectroscopy reveals NDI-T2 and not T-NDI-T to resemble the electronic structure of PNDIT2

Clemens Matt,^{a,b} Rukiya Matsidik,^{c,d} Deborah L. Meyer,^a Mirjam Schröder,^e
Michael Sommer,^d Till Biskup^{a,b,f,*}

^aInstitut für Physikalische Chemie, Albert-Ludwigs-Universität Freiburg,
Albertstraße 21, 79104 Freiburg, Germany

^bPhysikalische Chemie, Universität des Saarlandes,
Campus B2 2, 66123 Saarbrücken, Germany

^cInstitut für Makromolekulare Chemie, Albert-Ludwigs-Universität Freiburg,
Stefan-Meier-Straße 31, 79104 Freiburg, Germany

^dInstitut für Chemie, Polymerchemie, Technische Universität Chemnitz,
Straße der Nationen 62, 09111 Chemnitz, Germany

^eLeibniz-Institut für Katalyse e.V.,
Albert-Einstein-Straße 29a, 18059 Rostock, Germany

Present address: Bundesinstitut für Risikobewertung, Max-Dohrn-Straße 8–10, 10589 Berlin, Germany

Contents

Optical spectroscopy	2
EPR instrumentation	2
TREPR spectra of triplet states	3
Spectral simulations of TREPR spectra of triplet states	4
DFT calculations	6

*research@till-biskup.de

Optical spectroscopy

Absorption spectra were recorded using commercial UV/vis spectrometers (Shimadzu UV2450 and Analytik Jena SPECORD 210 PLUS) in combination with the corresponding software (UV-Probe version 2.43 and WinASPECT PLUS version 4.2.0.0). Cuvettes with a path length of 1 mm for T-NDI-T and 10 mm for NDI-T2 were used.

EPR instrumentation

TREPR spectroscopy with a time resolution of up to 10 ns allows for real-time observation, *e.g.*, of short-lived radical-pair and triplet states generated by pulsed laser excitation.[1–3] In contrast to conventional continuous-wave EPR spectroscopy, which usually involves magnetic-field modulation to improve the signal-to-noise ratio, TREPR is recorded in a high-bandwidth direct-detection mode, so as not to constrain the time resolution of the experiment. Consequently, positive and negative signal amplitudes in TREPR correspond to enhanced absorptive (A) and emissive (E) electron-spin polarisations of the EPR transitions, respectively.

TREPR experiments were performed at 80 K using similar experimental setups described below.

Setup 1 (NDI-T2)

The TREPR spectrum of NDI-T2 was recorded using a commercial EPR spectrometer (Bruker ESP380E) in conjunction with a Bruker microwave bridge (ER 046 MRT) equipped with a low-noise high-bandwidth video amplifier. The sample was placed in a synthetic-quartz (QSIL Ilmasil) sample tube (3 mm inner diameter) and irradiated in a dielectric-ring resonator (Bruker ER 4118X-MD5), which was immersed in a helium gas-flow cryostat (Oxford CF-935) cooled with liquid nitrogen. The temperature was regulated to ± 0.1 K by a temperature controller (Oxford ITC-503). The time resolution of the experimental setup was in the 10 ns range. A microwave frequency counter (Hewlett-Packard HP 5352B) was used to monitor the microwave frequency.

Optical excitation at the respective wavelengths was carried out with an optical parametric oscillator (OPO) system (Opta BBO-355-vis/IR) pumped by an Nd:YAG laser (Spectra Physics, Quanta Ray GCR 190-10) with a pulse width of approximately 6 ns, and a pulse energy of 1 mJ. The repetition rate of the laser was set to 10 Hz. As the residual polarisation of the laser beam is rather substantial, a quartz-wedge achromatic depolariser (Thorlabs DPU-25-A) was used.

A transient recorder (LeCroy 9354A) with a digitizing rate of 2 ns/11 bit was used to acquire the time-dependent EPR signal. To eliminate the background signal induced by the laser entering the EPR cavity, TREPR signals were accumulated at off-resonance magnetic-field positions (background) and subtracted from those recorded on-resonance. This background signal is completely independent in its shape from both, laser wavelength and magnetic field, and normally long-lived compared to the detected spin-polarised EPR signal. Background subtraction was performed directly in the transient recorder and a background signal repeatedly recorded after

each tenth time trace of the experimental data.

Further experimental parameters are as follows: Microwave frequency, 9.700 GHz, microwave power: 2 mW (20 dB attenuation, source power 200 mW), frequency-mixer detection, video amplifier set to 42 dB amplification and 25 MHz bandwidth, 800 averages per point.

Setup 2 (T-NDI-T)

The TREPR spectrum of T-NDI-T was recorded using a commercial EPR spectrometer (Bruker EMX) in conjunction with a Bruker microwave bridge (Bruker EMX premiumX). The sample was placed in a synthetic-quartz (QSIL Ilmasil) sample tube (3 mm inner diameter) and irradiated in a dielectric-ring resonator (Bruker ER 4118X-MD5), which was immersed in a closed-cycle cryostat (Cryogenic CF VTC) cooled with helium. The temperature was regulated to ± 0.1 K by a temperature controller (Lake Shore 350). The time resolution of the experimental setup was in the 300 ns range. The built-in microwave frequency counter was used to monitor the microwave frequency.

Optical excitation at the respective wavelengths was carried out with OPO system (GWU primoScan/BB/120-INDI) pumped by an Nd:YAG laser (Spectra-Physics Quanta-Ray INDI PS 51/52) with a pulse width of approximately 6 ns, and a pulse energy of 1 mJ. The repetition rate of the laser was set to 20 Hz. A transient recorder (Teledyne LeCroy HDO9204) with a digitizing rate of 2 ns/9 bit was used to acquire the time-dependent EPR signal. To eliminate the background signal induced by the laser entering the EPR cavity, TREPR signals were accumulated at off-resonance magnetic-field positions (background) and subtracted from those recorded on-resonance. This background signal is completely independent in its shape from both, laser wavelength and magnetic field, and normally long-lived compared to the detected spin-polarised EPR signal.

TREPR spectra of triplet states

As TREPR spectra of spin-polarised triplet states of organic molecules recorded at X-band frequencies and magnetic fields are normally dominated by the zero-field splitting (ZFS) interaction, the Hamilton operator used to describe the system reduces dramatically. The only contributions that need to be taken into account are the Hamilton operator for the Zeeman interaction, \mathcal{H}_{EZ} , and the one for the ZFS interaction, \mathcal{H}_{ZFS} :

$$\mathcal{H} = \mathcal{H}_{EZ} + \mathcal{H}_{ZFS} = \mathbf{g}\mu_B\vec{S}\vec{B} + \vec{S}\mathbf{D}\vec{S}. \quad (\text{S1})$$

All other contributions can be considered as small perturbations that can be accounted for using (inhomogeneous) line broadening.

The \mathbf{D} tensor in its principal axis system is given to

$$\mathbf{D} = \begin{pmatrix} -\frac{1}{3}D + E & 0 & 0 \\ 0 & -\frac{1}{3}D - E & 0 \\ 0 & 0 & \frac{2}{3}D \end{pmatrix} \quad (\text{S2})$$

where D and E are the zero-field-splitting parameters that can be directly read out from the experimental spectra (cf. Fig. S1). Note that D and E are defined such in the simulation routine used that the relation $|E| \leq |D|/3$ always holds. D can be described by:

$$D = \frac{3D_z}{2} = \frac{3}{4} \left(\frac{\mu_0}{4\pi} \right) (g_e \beta_e)^2 \left\langle \frac{r^2 - 3z^2}{r^5} \right\rangle, \quad (\text{S3})$$

with the distance between both unpaired electrons r . It can be correlated with the delocalisation length of the triplet exciton. A large value would mean a strong dipole-dipole interaction with a small distance between the electrons. The opposite is true for a small value of D .

Spectral simulations of TREPR spectra of triplet states

Processing and analysis of TREPR data was carried out using software written in MATLAB[®]. Preprocessing was carried out using the `trepr` toolbox.[4] All simulations of triplet spectra were performed using the `pepper` routine from the EasySpin software package [5]. Fitting was carried out using the `TSim` program developed by D. Meyer.[6, 7] Parameters included were the \mathbf{g} and \mathbf{D} tensor and the triplet sublevel populations (in zero field). Line broadening (Γ) was included using a combination of Lorentzian (Γ_L) and Gaussian (Γ_G) lines. For all simulations, the \mathbf{g} tensor was assumed to be isotropic, with $g_{\text{iso}} = 2.002$, and the population p_1 was set to zero. This left the parameters D and E of the zero-field splitting tensor \mathbf{D} , the populations p_2 and p_3 , and the two line widths Γ_L and Γ_G as the only free parameters that were adjusted. In the case of NDI the parameter E of the zero-field splitting tensor \mathbf{D} was set to zero and was not adjusted by a fitting process.

Fitting of the spectral simulations to the experimental data was performed by using the routine `lsqcurvefit` from the MATLAB[®] Optimization Toolbox[™] and here using the trust-region-reflective least squares algorithm.

The nonlinear least-square solver finds the m coefficients \vec{a} that solve the problem

$$\min_{\vec{a}} \sum_i (f(x_i; \vec{a}) - y_i)^2 \quad (\text{S4})$$

with y_i being the measured data and $f(x_i; \vec{a})$ the fitting function $f : \mathbb{R}^m \rightarrow \mathbb{R}^n$ with the same size n as the measured data y_i

Error estimation of the fitting parameters was carried out by using the Jacobian matrix \mathbf{J} . J_{ij}

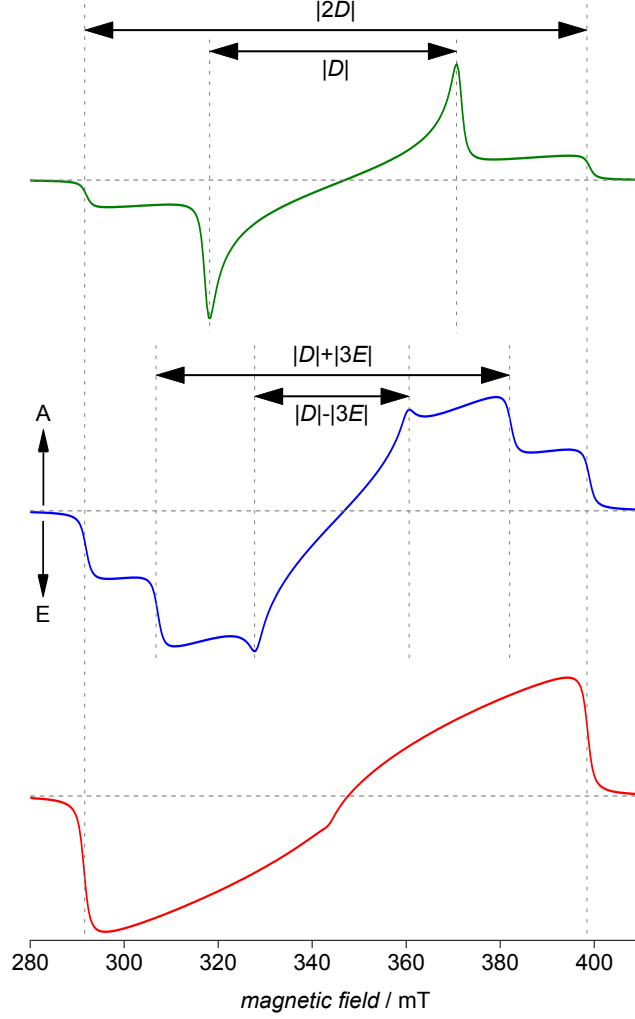


Figure S1: Characteristics of TREPR spectra of (photo-generated) spin-polarised triplet states. Three characteristic situations for the ratio of the two parameters D and E of the ZFS tensor are depicted here: the fully axial case (top, green), an intermediate case (blue, centre) and a fully rhombic case (red, bottom). Spectra were calculated using EasySpin. [2] The zero-field populations $p_{1,2,3}$ of the three triplet sublevels are far from thermal equilibrium, due to optical excitation and the inherent anisotropy of the intersystem crossing processes. Therefore, signals consist of both, enhanced absorptive (A) and emissive (E) contributions.

is the partial derivative of the fitting function $f(x_i; \vec{a})$ with respect to a_j at the solution \vec{a}_0 .

$$J_{ij}(\vec{a}_0) := \left(\frac{\partial f(x_i; \vec{a})}{\partial a_j}(\vec{a}_0) \right)_{i=1 \dots n, j=1 \dots m} \quad (\text{S5})$$

$$\mathbf{J}(\vec{a}_0) = \begin{pmatrix} \frac{\partial f(x_1; \vec{a})}{\partial a_1}(\vec{a}_0) & \dots & \frac{\partial f(x_1; \vec{a})}{\partial a_m}(\vec{a}_0) \\ \dots & \dots & \dots \\ \frac{\partial f(x_n; \vec{a})}{\partial a_1}(\vec{a}_0) & \dots & \frac{\partial f(x_n; \vec{a})}{\partial a_m}(\vec{a}_0) \end{pmatrix} \quad (\text{S6})$$

The variances of the coefficients a_j are given by the diagonal elements of the covariance matrix, \mathbf{C} , i.e. $\sigma_{a_j}^2 = C_{jj}$, where \mathbf{C} is the inverse of the matrix \mathbf{H} , variously referred to as the curvature or Hessian matrix.

The Hessian matrix was approximated by a series expansion, which is terminated after the first rank:

$$H_{jk} = \frac{1}{2} \frac{\partial^2 \chi^2(\vec{a})}{\partial a_j \partial a_k} \approx \sum_{i=1}^n \frac{1}{\sigma_i^2} \frac{\partial f(x_i; \vec{a})}{\partial a_j} \frac{\partial f(x_i; \vec{a})}{\partial a_k}$$

Hence the Jacobian matrix can be used to approximate the Hessian if σ_i^2 is chosen to be equal for all points,

$$\mathbf{H} \approx \frac{1}{\sigma_i^2} \mathbf{J}^T \cdot \mathbf{J}. \quad (\text{S7})$$

To speed up calculation time for the matrix product $\mathbf{J}^T \cdot \mathbf{J}$, an economy-size QR decomposition of \mathbf{J} was carried out, reducing the dimension of \mathbf{R} to the size of \vec{a} :

$$\mathbf{J} = \mathbf{Q} \cdot \mathbf{R}. \quad (\text{S8})$$

In the following matrix multiplication, \mathbf{Q} vanishes by multiplication with \mathbf{Q}^T :

$$(\mathbf{J}^T \cdot \mathbf{J})^{-1} = (\mathbf{R}^T \cdot \mathbf{R})^{-1} = \mathbf{R}^{-1} \cdot (\mathbf{R}^T)^{-1} = \mathbf{R}^{-1} \cdot (\mathbf{R}^{-1})^T \quad (\text{S9})$$

In MATLAB[®], this implementation leads to high computational speed and only minor numerical errors. The corresponding code would be as follows:

```
[~, R] = qr(jacobian, 0);
```

The diagonal elements of the approximated \mathbf{H}^{-1} can easily be calculated by element-wise squaring followed by summation over the rows of \mathbf{R} . Since σ_i^2 is chosen to be equal for all points, the errors for the fit parameters are given by:

```
stdDev = sqrt(variance * sum(inv(R).^2, 2));
```

The fitting algorithm `lsqcurvefit` can optionally return the residuals as additional output argument, here termed `residuals`. Hence the variance of the residuals obtained as

```
variance = var(residuals);
```

was used as σ^2 for all points.

DFT calculations

For T-NDI-T, NDI-T2, and the PNDIT2 fragment, different conformers have been considered that differ from each other in the orientation of the thiophene sulfur atom towards the O atom of the NDI unit. The results of the geometry optimisation of the singlet states, together with the energy differences, are depicted in Figs. S2 and S3. In each case, the conformer labelled ‘‘C1’’ with the lowest energy has been used for further calculations. For numerical values, see Tab. S1.

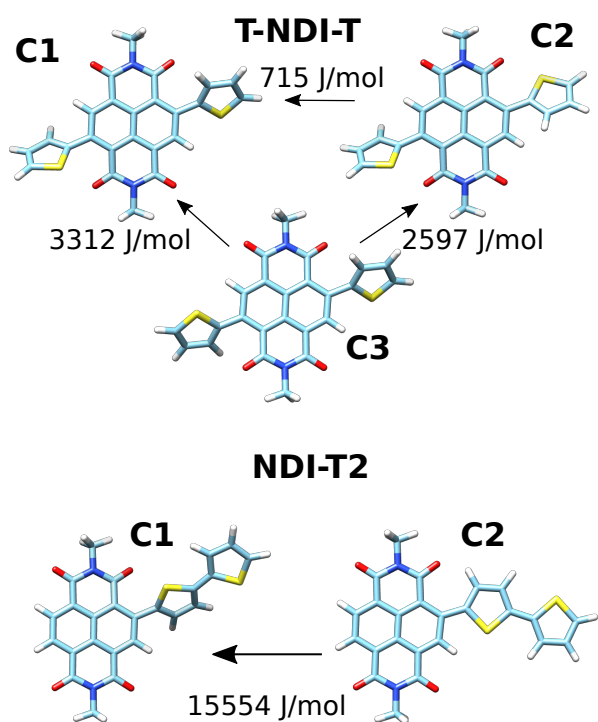


Figure S2: Different geometry-optimised conformers of the singlet ground state of NDI-T2 and T-NDI-T with their energy differences. The arrows point towards the conformation with lower energy. All geometries are optimised with the B3LYP functional and a 6-31G** basis set, together with a D3 dispersion correction.

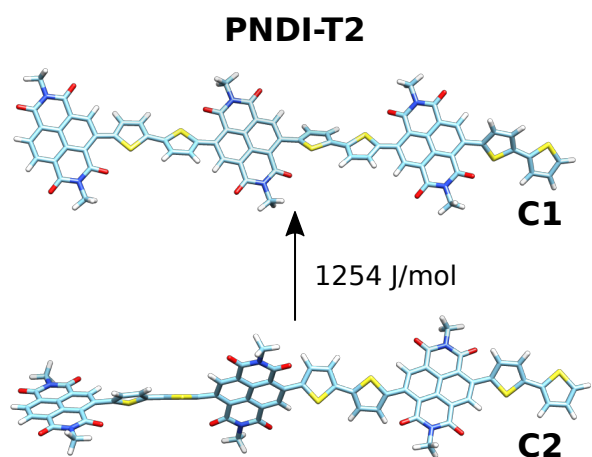


Figure S3: Different geometry-optimised conformers of the singlet ground state PNDI-T2 with their energy difference. The arrow points towards the conformation with lower energy. All geometries are optimised with the B3LYP functional and a 6-31G** basis set, together with a D3 dispersion correction.

Table S1: Energies of the singlet ground states of the different conformers. The energy differences ΔE were compared with the energy at room temperature $R \cdot T \sim 3300$ J/mol

Molecule	Conformer	Energy (Hartee)	Δ Conformers	ΔE (J/mol)
T-NDI-T	C1	-2129.065658519785	C2-C1	715
T-NDI-T	C2	-2129.064669405509	C3-C1	3312
T-NDI-T	C3	-2129.064396998741	C3-C2	2596
NDI-T2	C1	-2129.078349874169	C2-C1	15554
NDI-T2	C2	-2129.072425356022		
PNDI-T2	C1	-6384.857367446895	C2-C1	1254
PNDI-T2	C2	-6384.856889756274		

Similarly, spin densities for the triplet states of the different conformers have been calculated and are depicted in Fig. S4. Again, in the main text only the conformers with the lowest energy, labelled “C1”, are considered.

The labelling of the atoms used to plot the histogram of the Mulliken spin density in the main text is shown in Fig. S5.

References

- [1] M. D. Forbes, L. E. Jarocho, S. Sim, V. F. Tarasov, Time-resolved electron paramagnetic resonance spectroscopy: history, technique, and application to supramolecular and macromolecular chemistry, *Adv. Phys. Org. Chem.* 47 (2014) 1–83.
- [2] T. Biskup, Time-resolved EPR of radical pair intermediates in cryptochromes, *Mol. Phys.* 111 (2013) 3698–3703.
- [3] T. Biskup, Structure–function relationship of organic semiconductors: Detailed insights from time-resolved EPR spectroscopy, *Front. Chem.* 7 (2019) 10.
- [4] T. Biskup, B. Paulus, D. L. Meyer, trEPR toolbox, 2022. URL: <https://www.trepr.de/>. doi:10.5281/zenodo.7395548.
- [5] S. Stoll, A. Schweiger, EasySpin, a comprehensive software package for spectral simulation and analysis in EPR, *J. Magn. Reson.* 178 (2006) 42–55.
- [6] D. L. Meyer, F. Lombeck, S. Huettner, M. Sommer, T. Biskup, Direct $S_0 \rightarrow T$ excitation of a conjugated polymer repeat unit: unusual spin-forbidden transitions probed by time-resolved electron paramagnetic resonance spectroscopy, *J. Phys. Chem. Letters* 8 (2017) 1677–1682.
- [7] D. L. Meyer, T. Biskup, Tsim toolbox, 2022. URL: <https://tsim.docs.till-biskup.de/>. doi:10.5281/zenodo.7395749.

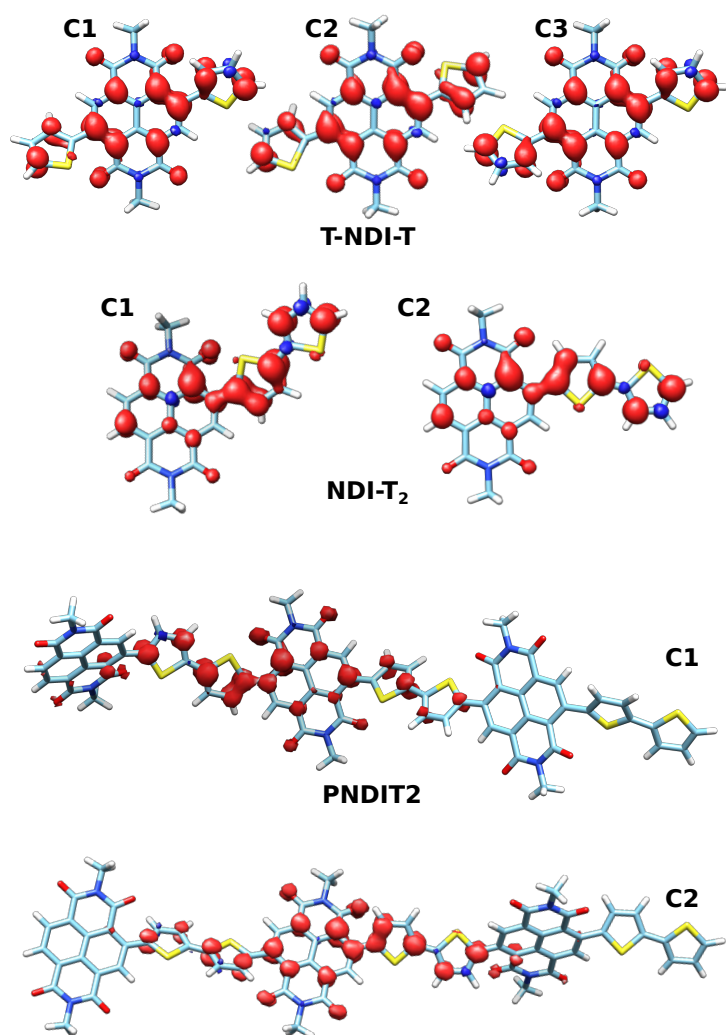


Figure S4: Calculated spin-density distribution for the two potential repeat units and the polymer fragment and their conformers. Geometries have been optimised for the triplet state with the B3LYP functional and 6-31G** basis set. Spin densities have been displayed for a threshold level of ± 0.003 , red denotes positive and blue negative spin density.

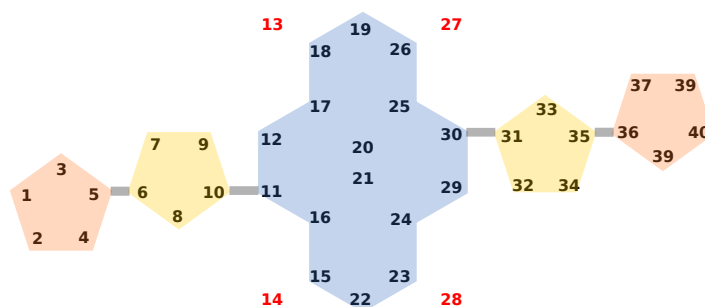


Figure S5: Atom labelling scheme for Fig 5 of the main text. The atoms were labelled from left to right, with T-NDI-T ranging from position 6 to 35 and NDI-T2 from 11 to 40.